The Gauls experienced the Roman Warm Period: Oxygen isotope study of the Gallic site of Thézy-Glimont, Picardie, France

Thibault Clauzel, Pascale Richardin, Jannick Ricard, Yves Le Béchennec, Romain Amiot, François Fourel, Brian Phouybanhdyt, Arnauld Vinçon-Laugier, Jean-Pierre Flandrois, Christophe Lécuyer

The Gauls experienced the Roman Warm Period: oxygen isotope study of the Gallic site of Thézy-Glimont, Picardie, France

Thibault Clauzel[a], Pascale Richardin[b,b'], Jannick Ricard[c], Yves Le Béchennec[c], Romain Amiot[a], François Fourel[d], Brian Phouybanhdyt[b,e], Arnauld Vinçon-Laugier[a], Jean-Pierre Flandrois[f] and Christophe Lécuyer[a,*, §]

a: Univ Lyon, Univ Lyon 1, ENSL, CNRS, LGL-TPE, F-69622, Villeurbanne, France

b: Centre de Recherche et de Restauration des Musées de France C2RMF, Palais du Louvre, Porte des Lions, 14 quai François Mitterrand, 75001 Paris, France

b': PRETECH – Préhistoire et Technologie, CNRS UMR7055, Université Paris Nanterre, Nanterre, France

c: TRAME (Université de Picardie Jules Verne) & Unité Mixte de Recherche n° 8546, AOrOc, CNRS, ENS Ulm, Paris, France

d: Laboratoire d'Ecologie des Hydrosystèmes Naturels et Anthropisés, CNRS UMR 5023, Université Claude Bernard, Lyon 1, France

e: GEOTRAC - Géochronologie Traceurs Archéometrie LSCE- Laboratoire des Sciences du Climat et de l'Environnement [Gif-sur-Yvette] : DRF/LSCE

f: Université de Lyon, CNRS, UMR 5558, Laboratoire de Biométrie et Biologie Evolutive, Villeurbanne, France

*: also at Institut Universitaire de France

§: corresponding author, email address: christophe.lecuyer@univ-lyon1.fr

Abstract (190 words)

The Roman Warm Period (from ≈300 BCE to ≈300 AD) is a climatic optimum, which had a key role in the development of the Roman civilization. This study provides new Mean Air Temperatures (MATs) inferred from the oxygen isotope composition of 80 bones and teeth apatite from 8 humans and 8 animals of the Gallic site of Thézy-Glimont, Picardie, France, dated between the 3rd and 2nd century BCE. Various bones from the cephalic, axial and

appendicular skeleton of three human individuals were sampled. All bones have similar phosphate $\delta^{18}O$ values for each individual, showing that the oxygen isotope signal of phosphate groups may be homogeneously recorded in bones. The sampled individuals were assumed to drink water from the nearby Avre river collecting local meteoric waters. The MATs were reconstructed combining (1) oxygen isotope fractionation equations between phosphatic tissues ($\delta^{18}O_p$) and drinking water ($\delta^{18}O_w$), and (2) relationships between MATs and $\delta^{18}O_w$. Depending on the used MAT-$\delta^{18}O_w$ relationship, the reconstructed MATs are 10.2°C±1.4°C and 10.5°C±1.7°C, which are comparable to present days (10.9°C). This study shows that the Gallic civilization also experienced relatively high temperatures since the initiation of the Roman Warm Period.

Keywords: oxygen isotopes; human skeleton; climate; Gauls, Roman Warm Period

1. Introduction

Although the Holocene is considered to be a very stable interglacial period, climatic variations from the centennial- to millennial-scale have been identified (Holzhauser et al., 2005; Caroli and Caldara, 2007; Lirer et al., 2014; Luterbacher et al., 2016; Cisneros et al., 2016). These variations are considered to be key elements in the rise and fall of civilizations. For instance, the Medieval Warm Period witnessed the development of rural populations in Europe linked to very productive harvests. Cities developed and major cultural innovations took place during warm periods due to land shortages and increasing food requirements (Fagan, 2008). On the other hand, at the end of the Late Bronze Age, most eastern Mediterranean urban centers were either destroyed or abandoned throughout the Middle East and the Aegean area. Some authors have recently suggested that a centuries-long

megadrought caused the widespread collapse of Bronze Age Palatial civilization (Kaniewski et al., 2010; Drake, 2012). The Roman Warm Period (RWP), also called the Roman Climatic Optimum or the Roman Humid Period, is a climatic variation of interest clearly identified in the European record. The RWP is identified as a key period for the development of the Roman culture all around the Mediterranean basin.

The concept of the RWP in Europe was first evoked by Lamb (1995) who provided a synthesis of archaeological, glaciological and palynological studies. The temporal definition of the RWP varies from one study to another, which may be due to the diversity of climate proxies and records in Europe. On average, its period extends between ≈300 BCE and ≈300 AD. The most direct proxies of the RWP are archaeological testimonies. Pliny the Elder (23-79 AD) testifies that, contrary to what had been the custom in earlier centuries, vines and olive trees were cultivated farther north in Italy. Ptolemy of Alexandria (100-168 AD) noticed that, around 140 AD, it rained every month of the year except August. McCormick et al. (2012) developed an online database referencing archaeological evidence of climate conditions during the Roman Period.

Although the RWP has been intensively studied in the European record, its climate characteristics remain unclear. Most of the studies of continental western Europe (essentially Spain, France and Italy) suggest a warm (e.g. McDermott et al., 2001; Roberts et al., 2001; Desprat et al., 2003; Holzhauser et al., 2005; Frisia et al., 2005; Berger and Bravard, 2012; Esper et al., 2012) and humid (e.g. Nesje et al., 2000; Wick et al., 2003; Ferrio et al., 2006; Magny et al., 2007; Migowski et al., 2006; Zanchetta et al., 2007) climatic episode.

All the studies reconstructing the level of the Dead Sea also suggest a humid episode (Frumkin et al., 1991; Heim et al., 1997; Bookman et al., 2004; Migowski et al., 2006). The data coming from coastal and marine sediments from all over the Mediterranean basin highlight a dry climate prevailing during the RWP (Schilman et al., 2001; Marquer et al.,

2008; Piva et al., 2008; Combourieu Nebout et al., 2009). This conflicts with the data coming from continental Europe presented above, and suggests that the Mediterranean basin was under the influence of a distinct climate regime during this episode.

High latitude records show a rather cold episode as documented in Iceland (Dahl-Jensen et al., 1998; Seidenkrantz et al., 2007). There are some records of a cold climate period in mid-latitudes, either in continental (Issar and Yakir, 1997; Baier et al., 2004; Mangini et al., 2005; Büntgen et al., 2011) or oceanic (Bond et al., 2001; Taricco et al., 2009; Wang et al., 2012; Lirer et al., 2014) environments. These temperature discrepancies may be explained by the existence of three cold and dry intervals during the RWP, which are named Roman I to III (Lirer et al., 2014; Margaritelli et al., 2016).

Variations of solar irradiance are currently invoked to explain the RWP (Bond et al., 2001; Jiang et al., 2005; Mangini et al., 2005; Wang et al., 2012). Some studies highlight correlations between solar activity variations and oceanic (Taricco et al., 2009; Lirer et al., 2014) or continental (Mangini et al., 2005; Margaritelli et al., 2016) records, suggesting that variations in solar activity may be the main mechanism responsible for the RWP. Dermody et al. (2012) have presented a model of a climatic "see-saw" between western/coastal Europe and Mediterranean/Eastern Europe, where solar activity variations trigger a change in the position and intensity of jet streams through thermal variations of the North Atlantic Ocean. However, these interpretations must be taken with caution, as the role of solar activity as a driver for climate variations is questionable and has been challenged in the last decades (e.g. Csiro, 1983; Haigh, 2007; Lockwood, 2012; Oldenborgh et al., 2013).

All the presented records suffer from significant dating uncertainties and, for most of them, are not focused on the RWP. No climatic reconstruction coming from human or animal bones is available so far for this period. This study aims to present stable isotope proxy records of Mean Air Temperature (MAT) inferred from vertebrate remains. Samples have

been collected from an archaeological site, well constrained in space and time, which is located in the North of France where an especially important lack of data has been noticed. The studied population belongs to the Gallic civilization. The Gauls, who came from Celtic populations, occupied most of Western Europe during the Iron Age (800 BCE – 50 BCE). Between the 2nd and 1st century BCE, the Roman Empire was involved in territorial conquests from minor Asia through Northern Africa and Greece to Western Europe, which includes Gallic territories. Therefore, the study of Gallic archaeological sites may bring information dealing with the transition from the Iron Age Cold Epoch and the RWP or the first part of the RWP, until ≈0 AD when all populations are expected to have been under the control of the Roman Empire.

The climate characteristics of the RWP can be studied at mid-to-low latitudes using the oxygen isotope composition of meteoric waters ($\delta^{18}O_{mw}$), which strongly depends on air temperature, humidity, the trajectories of humid air masses and the amount of precipitation (Dansgaard, 1964). Reconstructing the past $\delta^{18}O_{mw}$ variations of meteoric waters permits an estimation of the past variations of those climate parameters.

It is known that the oxygen isotope composition of phosphate group ($\delta^{18}O_p$) from mineralized tissues of mammalian individuals (bones, teeth) is related to the oxygen isotope composition of drinking water ($\delta^{18}O_w$) (Longinelli, 1984; Luz et al., 1984; Luz and Kolodny, 1985; Kohn, 1996). During pre-industrial times, most of the consumed water came from local sources (wells, springs, nearby watercourses), which are derived from local meteoric waters (Daux et al., 2005; Darling, 2006). The contribution of water from food varies from one species to another, according to the water-turnover of the animal (Kohn, 1996). Water turnover scales to body-mass for most terrestrial vertebrates (Eberhardt, 1969). Humans are medium omnivores with moderate water turnover, around 5 to 10% of total body water per day (Shimamoto and Komiya, 2000), which means that the $\delta^{18}O$ of water ingested is strongly

and mainly imprinted by the $\delta^{18}O$ of drinking water. The cooking operation of brewing or stewing may lead to an isotopic enrichment of the water contained in food compared to meteoric water (Brettell et al., 2012), but its effect is not unanimous (e.g. Daux et al., 2008).

Therefore, measuring the oxygen isotope composition of phosphatic tissues from terrestrial mammalians allows the $\delta^{18}O_{mw}$ of contemporary meteoric waters to be calculated, hence climate parameters such as MAT to be quantified. We demonstrate in this study that the reconstructed MATs at Thézy-Glimont were similar to those of today.

2. Material and methods

2.1. The Gallic site of Thézy-Glimont

The Gallic site of Thézy-Glimont is located in the Valley of the Somme, in the region of Picardie, France, 15 km southeast from the city of Amiens. (Figure 1). The site was excavated in the context of rescue archaeology by the Service d'Archéologie Préventive Amiens Métropole (SAAM) between November 2012 and May 2013 (Le Béchennec et al., 2016).

Picardie is located at mid-latitude (49°N-50°N) in the northwest of Europe, climatically under the prevailing fresh and humid westerlies from the North Atlantic Ocean. The climate is rated as Cfb (warm temperate, fully humid with warm summers) according to the Köppen-Geiger classification (Kottek et al., 2006) with a yearly average temperature of 10.9°C and a small seasonality amplitude of ±5.4°C throughout the years 1980 to 2010 (data from Météo France™). The yearly precipitation rate is 631 mm, with a small seasonality amplitude of ±7 mm, July and December being the two most humid months.

Thézy-Glimont (49°48'N – 2°25'E) is located at the bottom of the Avre Valley, which is a tributary of the Somme river. The Avre river is assumed to have been the drinking water

153 source of the inhabitants of Thézy-Glimont as it is located on the edge of the archaeological
154 site and no water wells have been observed.

155 The SAAM highlighted 17 rectangular graves during the excavation. The graves contain
156 horses (*Equus caballus*), bovids (*Bos taurus*) and a human (*Homo sapiens*) for most of them.
157 Sometimes a pig (*Sus scrofa*) has been found. All deposits seem to be intentional and
158 organized. They were filled with the same sediment (white chalk) coming from the digging,
159 whereas the tradition of Gallic funeral practices is usually cremation. The excavation report
160 chooses to present the graves as "offering graves", even if their true nature is not fully
161 understood (Le Béchennec et al., 2016). A total of 8 human, 12 horse, 39 bovid and 3 pig
162 skeletons were excavated from the 17 graves.

163 All 8 humans, 2 horses, 5 bovids and 1 pig were sampled from this corpus (see Table 1).
164 A great number of sampled individuals come from TGV 1135 as it was the first grave to be
165 excavated, the biggest of the archaeological site and the one with the highest number of
166 individuals. The humans are all young males without any noticeable disease. The human
167 identified as sample TG-02 is the youngest, around 15 years old, while TG-05 is the oldest
168 (between 30 and 59 years old). The forensic expertise suggested a quick burying after death
169 before the rigor mortis happened. Although the

170 Eighty samples (bones and teeth) were collected (Table 1). Bone samples were collected
171 using a toothless diamond saw blade fitted to a Dremel™ drill. Various elements coming
172 from the axial, cephalic and appendicular skeletons of TG-01, TG-02 and TG-03 were
173 sampled along with 19 bones for TG-01, 14 for TG-02 and 19 for TG-03, respectively (Figure
174 2). The bone samples were first abraded using a surgical knife in order to remove the altered
175 layer at the surface and grossly crushed using a hammer. All samples were washed with
176 acetone to degrease them, rinsed three times with Ultrapure™ water and dried in an oven
177 under medium vacuum, at 60°C, for 24 hours. Clean samples were then crushed in fine

178 powder using a Pulverisette 7^{TM} planetary ball mill composed of zirconium oxide. Teeth were
179 extracted from the skulls by gently pulling them from their sockets. They were rinsed with
180 Ultrapure^{TM} water and cleaned using a toothbrush. The powder was obtained by drilling the
181 enamel of the teeth with a Dremel^{TM} diamond-head drill bit.
182
183 *2.2. Dating of the archaeological site*
184
185 During the excavation of the archaeological site, Beta Analytics^{TM} realized ^{14}C datings
186 on 13 samples, giving dates with 68.3% probability (1σ) between 200 BCE and 5 AD. New
187 ^{14}C dates were realized on collagen extracted from 7 human, 2 horse and 1 bovid bones. The
188 protocol of the extraction of soluble collagen was based on the method described by Longin
189 (1971) and has been previously described in detail by Richardin et al. (2017).
190 All measurements were performed with Accelerator Mass Spectrometry techniques
191 from the Artemis AMS facility at Saclay (France) (Moreau et al., 2013). Calendar dates were
192 determined using the OxCal v.4.2 procedure and the most recent calibration curve data for the
193 Northern Hemisphere, IntCal13 (Reimer et al., 2013). Calibration of radiocarbon ages was
194 performed considering that the contribution of marine products to the diet of the Gauls
195 remained marginal. Calibrated date ranges (Table 1) correspond to 95.4% probability (2σ).
196 The archaeological site is dated with 95.4% certainty between 350 BCE and 60 BCE with the
197 highest probability being between 350 BCE and 200 BCE, one century earlier than previously
198 proposed. There are no obvious differences among and between the humans and the animals,
199 therefore all the graves seem contemporary, their digging possibly spread over a century.
200
201 *2.3. Bone turnover and isotope homogeneity*
202

The bone tissue is vascularized, composed at 60 to 70% of hydroxyapatite crystals tightly inter-grown with an organic matrix predominantly composed of type I collagen for 20 to 30%. Several ion substitutions can be observed in the crystalline matrix (LeGeros, 1981; Wopenka and Pasteris, 2005). Enamel from teeth has much larger bioapatite crystals and a very low organic content, which makes it less sensitive to diagenesis (Tütken and Vennemann, 2011). Bone and tooth formation starts in the embryo, but human teeth complete accretion long before bone growth has finished. The human permanent dentition is expected to be fully formed at about 12 years, while a complete bone structure can be achieved at the age of 20. Tooth enamel and dentine grow by accretion and do not renew afterwards. On the contrary, there is a set-up of re-absorption of old bone (both organic and inorganic matrix) and deposition of new bone tissue. At maturity, this mechanism happens to be continuous and the bone is said to "turnover". For a young adult, the total bone tissue is expected to turnover every five to six years, although it may depend on the bone region or the individual health status (Glimcher, 2006). Therefore, the stable isotope composition of the bone tissue only represents the last 5 to 10 years of the individual life, while that of a tooth will represent the first 12 years of life. Some studies use the discrepancy of bone turnover to highlight a change of the diet (e.g. Lamb et al., 2014).

Because of poor conservation of the material in the field, the lack of articulations between bones or the preciosity of samples, most isotope studies on bone material are realized on one bone (generally the femur or the rib) and assume the value is representative of the whole individual characteristics (e.g. Prowse et al., 2004; Jay and Richards, 2006). However, if bone turnover is highly variable at the intra- and inter-individual scale, we can wonder to what extent the isotope study of one bone is representative of the whole skeleton? To investigate this issue, several parts (bones and teeth) of the same skeleton have been sampled from the three best conserved and most complete skeletons of human individuals (TG-01, TG-

02 and TG-03) excavated in Thézy-Glimont (see Figure 2). Intra-comparisons of the oxygen isotope composition of mineralized tissues were realized for each individual.

2.4. Oxygen isotope ratios of apatite phosphate

Oxygen isotopic analyses were performed with stable isotope mass spectrometry techniques. Phosphate ions were extracted from the apatite using a wet chemistry procedure. After the dissolution of about 30 mg of each sample in 2 mL of 2M HF at ambient temperature for 24 hours, the CaF_2 precipitate was separated from the sample solution by centrifugation. The phosphate ions were neutralized with KOH and isolated using a strong anionic resin (Amberlite IRN 78) before being precipitated as silver phosphate following the method first described by Crowson et al. (1991) and slightly modified by Lécuyer et al. (1993). The oxygen isotope data were obtained using a high-temperature pyrolysis continuous flow technique developed by Lécuyer et al. (2007) and Fourel et al. (2011). For each sample, five aliquots of 400–500 μg of silver phosphate were mixed with 500 μg of carbon loaded into 3.5x5 mm silver foil isotope grade capsules (Eurovector™). Pyrolysis was performed at 1450°C using a PYROcube™ elemental analyzer (Elementar GmbH-Germany) interfaced in continuous flow mode with an isotopic ratio mass spectrometer Isoprime™ (Elementar UK Ltd UK). Measurements were performed with CO gas separated by purge and trap technology within the PYROcube™ system at the Laboratoire de Géologie de Lyon and at the Laboratoire d'Ecologie des Hydrosystèmes Naturels et Anthropisés, both hosted by the Université Claude Bernard Lyon 1. The official unit for isotopic ratios is the Urey (Ur), although the unit commonly used is the permil (‰, 1‰ = 1mUr). For practical reasons, data are reported as $\delta^{18}O$ values with respect to V-SMOW in ‰ units.

252 Oxygen isotope compositions were drift corrected to account for instrumental
253 variations. Results were calibrated against silver phosphate samples of known $\delta^{18}O$ values
254 precipitated from the NBS120c standard for which the $\delta^{18}O$ value was fixed at 21.7‰ (V-
255 SMOW) (Lécuyer et al., 1993; Chenery et al., 2010; Halas et al., 2011), as well as with
256 NBS127 (barium sulfate) having a certified value of 9.3‰ (V-SMOW) (Hut, 1987). NBS120c
257 standards were converted into silver phosphate along with the samples from each chemistry
258 batch and considered as "internal standards". They have $\delta^{18}O$ values that range from 21.4‰
259 to 22.2‰ with a mean value of 21.76±0.25‰ (*n*=12). The analytical uncertainty for samples
260 is always lower than 0.3‰ (2σ).
261
262 **3. Results**
263
264 *3.1. Intra-skeletal variability of the $\delta^{18}O_p$ from human bones*
265
266 The intra-skeletal variability of the $\delta^{18}O_p$ values from the three human individuals
267 TG-01, TG-02, TG-03 range from 16.1‰ to 16.9‰ with a mean value of 16.6‰ for TG-01,
268 from 17.4‰ to 17.9‰ with a mean value of 17.6‰ for TG-02 and from 16.4‰ to 17.3‰
269 with a mean value of 16.8‰ for TG-03 (Figure 2). The standard deviation, representing the
270 intra-skeletal variability of oxygen isotope composition, is respectively 0.2‰, 0.2‰ and
271 0.3‰ for TG-01, TG-02 and TG-03. Local deviations of bones $\delta^{18}O_p$ from the average
272 skeleton $\delta^{18}O_p$ value has been calculated for each individual as follows:
273

$$\delta^{18}O^{bone}_{skeleton}(‰) = \delta^{18}O^{bone}_{V-SMOW} + \delta^{18}O^{V-SMOW}_{skeleton} + \delta^{18}O^{bone}_{V-SMOW} \times \delta^{18}O^{V-SMOW}_{skeleton} \times 10^{-3}$$

274

No localized and repeatable enrichment or depletion in ^{18}O relative to the average $\delta^{18}O_p$ value is observed among the three individuals.

3.2. Oxygen isotope values of phosphatic tissues

The oxygen isotope compositions of apatite phosphate from the 80 samples were analyzed (Figure 3, Supplementary Table 1). The $\delta^{18}O_p$ values of human bones and teeth range from 15.1‰ to 18.0‰. Teeth are systematically enriched in ^{18}O relative to bones by respectively 0.9‰, 0.3‰ and 0.9‰ for TG-01, TG-02 and TG-03. Human bones have a mean $\delta^{18}O_p$ value of 16.2‰ with a standard deviation of 0.8‰. TG-02, who is the youngest analyzed individual, is significantly enriched by 1.3‰ compared to the other humans. The analyzed pig has a mean $\delta^{18}O_p$ value of 15.6‰ with a standard deviation of 0.5‰. The bones from 5 bovids have a mean $\delta^{18}O_p$ value of 17.3‰ with a standard deviation of 0.2‰, while the two teeth from individuals TG-B4 and TG-B5 have a mean value of 16.1‰ and a standard deviation of 0.1‰. Teeth are significantly depleted in ^{18}O by 1.3‰ relative to bones. No significant isotopic difference is observed relative to sex (TG-B1 versus the others) or to the grave the individuals were buried in (TG-B5 versus the others). Molars from the two horses have a mean value of 15.8‰ with a standard deviation of 0.6‰. In the case of the horse TG-CH1, the bone $\delta^{18}O_p$ value is 1.4‰ higher than that of the tooth. The bones of herbivores (horse, bovid) have a mean $\delta^{18}O_p$ of 17.5‰, while the average $\delta^{18}O_p$ for omnivores (human, pig) is 15.9‰.

4. Discussion

4.1. Sample preservation and diagenesis

The bones from Thézy-Glimont showed a visible brownish layer of alteration, which was removed using a surgical knife. Some of the human teeth showed attrition, which is a common feature for the gallic civilization. It may be due to the habit of eating gritter bread containing sediment particles. Attrition may have altered mechanically the teeth without scrambling the isotopic signal recorded in enamel.

In apatite, P-O bond is known to be very resistant to inorganic isotope exchange with aqueous fluids at surface temperatures (e.g. Blake et al., 1997; Lécuyer et al., 1999). No trace of microbially induced diagenesis has been detected. An expected offset of the $\delta^{18}O_p$ signal between teeth and bones from the same individual has been noticed (Touzeau et al., 2013; Martin et al., 2017). All three individuals TG-01, TG-02 and TG-03 have very low $\delta^{18}O_p$ intra-skeletal variability (Figure 2). When considering all the measurements from each skeleton the three standard deviations of 0.2‰, 0.2‰ and 0.3‰, respectively, are in the same order of magnitude as the analytical uncertainty (±0.3‰). No noticeable and localized isotopic enrichment or depletion relative to the average $\delta^{18}O_p$ value has been noticed. All these observations support the hypothesis of the preservation of the pristine oxygen isotope compositions of phosphatic tissues.

4.2. Homogeneity of oxygen isotope values in human skeleton apatite phosphate

The mapping of the oxygen isotope composition of human bone apatite at the skeletal level of observation (Figure 2) revealed that, in the case of $\delta^{18}O_p$ values, the study of one selected bone is representative of the composition of the whole individual. We observe an isotopic homogeneity at the skeleton scale, although the bones have various turnover rates. Two complementary explanations are proposed: TG-01, TG-02 and TG-03 being young, they

might have only realized one cycle of bone turnover at most and their diet did not change during this interval of time. As migrations can be recorded by apatite $\delta^{18}O_p$ values (e.g. Lightfoot and O'Connell, 2016), we also propose that they were sedentary and lived all their life in Picardie, France, which could be confirmed with supplementary analysis such as the use of strontium isotopes. The oxygen isotope variability inside a bone has not been investigated, but the epiphysis of some bones (e.g. the humerus) and the diaphysis of others (e.g. the tibia) were analyzed and no noticeable offset was detected. With caution, following studies of the oxygen isotope composition of bones in archaeological sedentary populations may assume that one bone is representative of the whole individual. The $\delta^{18}O_p$ value of vertebrates is also dependent on body temperature (Kohn, 1996) and has been used to study the thermophysiology of terrestrial (Barrick and Showers, 1994, 1995; Amiot et al., 2006) and marine vertebrates (Bernard et al., 2010; Séon et al., 2020). Thermal variations (or regional heterothermy), which exist at a human body scale, are not documented at the light of our study of the oxygen isotope ratios of phosphatic tissues.

4.3. The $\delta^{18}O_p$ record in teeth and bones from individuals of Thézy-Glimont

There is a very low $\delta^{18}O_p$ variability observed between humans and animals from Thézy-Glimont. The $\delta^{18}O_p$ values from herbivore bones are on average 1.7‰ higher than those from omnivorous individuals. This can be explained by the diet of the herbivores mainly eating grass and leaves containing water which is ^{18}O-enriched in relation to the plant evaporative system (Barbour, 2007). Comparing the oxygen isotope value from herbivores and omnivores (mainly humans) enables to address the question of the influence of food processing on $\delta^{18}O_p$. Although no information is available about the dietary practices on this archaeological site, stewing or brewing may be detected through an isotopic enrichment of

body water later translated in a higher $\delta^{18}O_p$ of human bones compared to herbivores (Brettell et al., 2012). This effect is not detected in this study, which leads to two possible conclusions: either the inhabitants of Thézy-Glimont had dietary practices which did not include brewing or stewing, or these cooking processes are not detected in the oxygen isotope composition of bone apatite. This latter conclusion agrees the works of Daux et al., (2008) on modern human teeth samples and Chesson et al. (2010) on the similarity of oxygen isotope values of different modern beverages and meteoric waters in a same location.

The $\delta^{18}O_p$ value of human teeth enamel is higher than the $\delta^{18}O_p$ value of bones, especially for TG-01 (+0.9‰) and TG-03 (+0.9‰). These values are comparable to the offset between infant and adult bones of ≈+1.2‰ found by Britton et al. (2015) which can be attributed to a specific diet during childhood. A large part of the child's diet consists of milk, which is ^{18}O-enriched from the mother's body water. The second and third molars, respectively M2 and M3, are considered post-weaning teeth and do not record any breast-feeding. Although the M3 is not discernable from the oxygen isotope value of bones from TG-02 and is ^{18}O-depleted compared to the two other teeth for TG-03, the M2 has similar values than pre-weaning teeth (M1 for TG-01 and PM1 for TG-03). On the contrary, herbivore teeth are depleted in ^{18}O compared to bones: -1.3‰ for bovids and -1.4‰ for the horse TG-CH1. Herbivore hypsodont teeth, which grow continuously and are often used to study climate seasonality (e.g. Bernard et al., 2009), record a signal which is more limited in time than bones. For the last decade, the average interannual change in yearly MAT of Picardie, France, is ±1°C (data from historique-meteo.net) and can go as high as 2 – 2.5°C (for instance between 2013 and 2014). Translated into $\delta^{18}O$ of local meteoric waters, this interannual change is ±0.6‰ on average and can go as far as a ±1.6‰, which is in the range of the teeth-bones offset noticed for the herbivores. We propose that herbivore teeth recorded more time-limited interval and colder climatic conditions, hence presenting an offset from the

bones $\delta^{18}O$ record, which represents a pluriannual time scale. Bones are a better material to reconstruct MAT on the pluriannual time scale than teeth which record either a drinking water environmental signal mixed with breastfeeding in the case of humans or a time-limited signal in the case of herbivores. Therefore, only the oxygen isotope values coming from bones are considered for the calculation of $\delta^{18}O_w$ of drinking water and MATs reconstruction.

TG-02 is ^{18}O-enriched compared to all the other humans and there is no significant difference between the $\delta^{18}O_p$ of his bones and his teeth (see Figure 3). This isotopic offset can be attributed to his young age (estimated at 15 years) keeping in mind that the set-up of bone turnover is only achieved around 20 years-old. The bones from TG-02 might still record a residual signal from the breast-feeding period, mixed with a signal coming from drinking water. Therefore, this individual was removed from the reconstruction of the $\delta^{18}O$ of environmental drinking water.

The oxygen isotope composition of phosphatic tissues from individuals with a medium to low water turnover is mostly representative of the $\delta^{18}O$ of the drinking water. Thézy-Glimont is located in a valley bottom, a few meters away from the Avre river, which is assumed to be the main drinking water source of local inhabitants. The $\delta^{18}O_p$ record is, therefore, representative of the climate parameters linked to the Avre river. The relationship between the $\delta^{18}O_p$ of phosphatic tissues and the $\delta^{18}O_w$ of drinking water has been determined empirically in numerous groups of vertebrates. These oxygen isotope fractionation equations mainly depend on the basal metabolism, body mass and diet (herbivorous vs. carnivorous vs. omnivorous) of species. Several equations have been used in this study and are represented in Figure 4 as follows:

Daux et al. (2008) for humans:

$$\delta^{18}O_w(\pm 1.51‰) = 1.54 \times \delta^{18}O_p - 33.72$$

400

401 Longinelli (1984) for pigs:

402

$$\delta^{18}O_w = \frac{\delta^{18}O_p - 22.71}{0.86}$$

403

404 D'Angela and Longinelli (1990) for bovids:

405

$$\delta^{18}O_w = \frac{\delta^{18}O_p - 24.90}{1.01}$$

406

407 Bryant et al. (1994) for equids:

408

$$\delta^{18}O_w(\pm 2.46‰) = \frac{\delta^{18}O_p - 22.90}{0.6863}$$

409

410 The errors associated with the linear regression of empirical data (y = mx + b) have
411 been computed as the mean standard error for the "y" value when not available in the original
412 publication and are ±0.2‰ for the equation of Longinelli (1984) and ±0.1‰ for the equation
413 of D'Angela and Longinelli (1990). We highlight that these uncertainties may be
414 underestimated as both of the isotope fractionation equations have been established with a
415 very low number of data, respectively 7 average $\delta^{18}O$ values for Longinelli (1984) and 5
416 average $\delta^{18}O$ values for D'Angela and Longinelli (1990).

417 Using these equations, $\delta^{18}O_p$ were converted into $\delta^{18}O_w$ values (Figure 4,
418 Supplementary Table 2), which were interpreted as reflecting the oxygen isotope composition
419 of the Avre river during the 2nd to 3rd century BCE. The mean $\delta^{18}O_w$ inferred from humans

and animals is -8.4‰, with a standard deviation of ±1‰. The propagation of uncertainty, represented as error bars in Figure 4, have been calculated as the quadratic sum of the analytical uncertainty, errors associated with the equations and variability in the case of several measurements obtained for a single individual (TG-01, TG-02, TG-03 and TG-C1). Taking into account these uncertainties, all the $\delta^{18}O_w$ values are homogenous and we can affirm that they represent one main water source.

The present-day isotopic composition of the Avre river water was measured by Négrel and Petelet-Giraud (2005) twice in a year (Avril and October 2001), with respective $\delta^{18}O_w$ values of -6.86‰ and -7.00‰. The $\delta^{2}H$ and $\delta^{18}O$ values of the Avre river match the Global Meteoric Water Line (Craig, 1961) as well as the Brest-Orléans isotopic rainwater domain, confirming that the signal from the Avre river reflects the composition of local meteoric waters. The oxygen isotope composition of meteoric waters is dependent on temperature, rate of precipitation and the trajectory of humid air masses (Craig and Gordon, 1965; Rozanski et al., 1993; Gat, 1996). During the last two millennia, the climatic moisture delivered through Europe has been driven by the North Atlantic Oscillation (NAO) (Smith et al., 2016) and it is reasonable to consider that there has not been any major change in the balance between the water cycle reservoirs for this interval of time (Darling, 2006). For mid- to high-latitudes, rough linear correlations are observed between the $\delta^{18}O$ of meteoric water and air temperature (e.g. Dansgaard, 1964; Rozanski et al., 1992; Fricke and O'Neil, 1999). Such correlations result from isotopic compositions that obey a Rayleigh distillation law in both evolving reservoirs of vapor water and condensed water. Condensation in clouds globally proceeds from warm low latitudes toward cold high latitudes. Air temperature in the residual clouds tends to decrease resulting in an increasing isotopic difference between precipitation and water vapor.

For Europe, the slope between $\delta^{18}O_{mw}$ and Mean Air Temperature (MAT) is considered to be 0.58‰ per °C (Rozanski et al., 1992). We combine the $\delta^{18}O_w$ (now assumed to be local $\delta^{18}O_{mw}$) obtained from measurements performed on individuals from Thézy-Glimont to relationships between $\delta^{18}O_{mw}$ and MATs. Several relationships (Dansgaard, 1964; Rozanski et al., 1992; Fricke and O'Neil, 1999; von Grafenstein et al., 1996; Lécuyer, 2013) are available in the literature. These different equations may provide sizeable differences in the calculated air temperature (Daux et al., 2005). We chose two equations we considered the most appropriate in the framework of this study. First, the equation provided by von Grafenstein et al. (1996), which has been established at Lake Ammersee, Bavaria, Germany (48°00'N - 11°07'E), only located ≈2° of latitude south of Thézy-Glimont. The equation is expressed as follows:

$$MAT\ (°C) = \frac{\delta^{18}O_{mw} + 14.48}{0.58\ (\pm 0.11)} \quad (1)$$

Secondly, we also considered the isotope fractionation equation established by Lécuyer (2013) as it has been constructed from European meteorological stations excluding those from the Mediterranean basin, which is under the influence of a specific climatic mode (Lécuyer et al., 2018). The equation is expressed as follows:

$$MAT\ (°C) = 1.41\ (\pm 0.09) \times \delta^{18}O_{mw} + 22.02\ (\pm 0.83) \quad (2)$$

A reconstruction of mean annual $\delta^{18}O_{mw}$ value at the location of Thézy-Glimont (49°N, 2°E) using The Online Isotopes in Precipitation Calculator (Bowen and Revenaugh, 2003; IAEA/WMO, 2015; Bowen, 2020) gives a value of -6.7±0.2‰, which is very close to the

April (-6.86‰) and October (-7.00‰) $\delta^{18}O_w$ values measured on the Avre river by Négrel and Petelet-Giraud, (2005). We emphasize that at mid latitudes, sinusoidal-like seasonality in meteoric water $\delta^{18}O_{mw}$ values mathematically leads to spring and autumn $\delta^{18}O_{mw}$ values matching the mean annual one. Therefore, we use these inter-season oxygen isotope values to test both $\delta^{18}O_{mw}$-MAT equations for the Picardie region. The calculated temperatures are 13.1±1.6°C and 12.3±1.6°C in April and 12.9±1.6°C and 12.1±1.6°C in October for equations (1) and (2), respectively. The isotope data from April 2001 may be biased as floods happened in the Somme department during this month, which led to an ^{18}O enrichment of the Avre river water sampled for the study. As far as October data are concerned, the calculated temperatures are near the average temperature of 11.6°C for this month (data from Météo France^{TM}). Those results indicate that both equations are reliable to infer MAT from $\delta^{18}O_{mw}$ and could safely be applied to the late Iron Age.

When applying equations (1) and (2) to the calculated $\delta^{18}O_{mw}$, the reconstituted air temperatures for the late Iron Age are on average 10.5°C±1.7°C for equation (1) and 10.2°C±1.4°C for equation (2) (Figure 5). Therefore, the results for both of these equations being very close, those calculated MATs are ascribed to Thézy-Glimont during the 3rd to 2nd century BCE. These calculated MAT well compare the present-day average temperature of 10.9°C recorded in Amiens, Picardie. Our result implies that mid-latitudes also experienced a climate optimum that can be attributed to the RWP, with continental temperatures close to present-days. This MAT is consistent with results obtained from other studies realized at mid-latitudes, such as palynological data from Tinner et al. (2003), sedimentological data from Holzhauser et al. (2005) and geochemical data obtained from speleothems by McDermott et al. (2001).

We assign such mild air temperatures to what is considered to be the initiation of the RWP. The timing of the RWP is still unsure as well as its climatic characteristics. There may

always remain some discrepancies in the European temperature record for the RWP because no global coherent warm period has occurred on Earth (Neukom et al., 2019) excluding the current climate change. Nonetheless, this study provides a new climatic anchor point which is well constrained in space and time, in a region lacking climatic data for the RWP.

5. Conclusion

The Gallic site of Thézy-Glimont provides an insight into the climatic conditions occurring during the 3rd to 2nd century BCE in the North Gaul. An oxygen isotope mapping of three human skeletons revealed a great homogeneity of $\delta^{18}O_p$ values within the range of analytical uncertainty. This result is of paramount importance in archaeological studies as it means that, in the case of $\delta^{18}O_p$ values of sedentary populations, the use of one bone as representative of the whole skeleton is justified.

The $\delta^{18}O_p$ of bones from Gauls and associated animals record the $\delta^{18}O$ value of drinking water, which illustrates the climatic conditions prevailing in Picardie, France. The reconstructed air temperatures are 10.2°C±1.4°C and 10.5°C±1.7°C depending on the selected $\delta^{18}O_{mw}$-MAT equation. Here, we emphasize that those estimated mean air temperatures are similar to present-day ones. Mild air temperatures recorded in Picardie, France, during the beginning of the RWP is a new result that needs to be taken into consideration for understanding the climatic regime of the RWP in Europe. This study also shows that archaeological artefacts may provide quantified climatic anchor points with a high spatial and temporal resolution, playing a key role in our knowledge of the Late Holocene short-term climatic changes.

Declaration of competing interest

The authors declare that they have no known competing financial interests or personal relationships that could have appeared to influence the work reported in this paper.

Acknowledgments

This study was funded by the Centre National de la Recherche Scientifique and the Institut Universitaire de France (CL). We thank the SAAM and its director Josabeth Millereux- Le Béchennec for providing the archaeological samples presented in this study.

References

Amiot, R., Lécuyer, C., Buffetaut, E., Escarguel, G., Fluteau, F., Martineau, F., 2006. Oxygen isotopes from biogenic apatites suggest widespread endothermy in Cretaceous dinosaurs. Earth and Planetary Science Letters 246, 41–54. https://doi.org/10.1016/j.epsl.2006.04.018

Baier, J., Lücke, A., Negendank, J.F., Schleser, G.-H., Zolitschka, B., 2004. Diatom and geochemical evidence of mid-to late Holocene climatic changes at Lake Holzmaar, West-Eifel (Germany). Quaternary international 113, 81–96.

Barbour, M.M., 2007. Stable oxygen isotope composition of plant tissue: a review. Functional Plant Biol. 34, 83–94. https://doi.org/10.1071/FP06228

Barrick, R.E., Showers, W.J., 1995. Oxygen isotope variability in juvenile dinosaurs (*Hypacrosaurus*): evidence for thermoregulation. Paleobiology 21, 552–560. https://doi.org/10.1017/S0094837300013531

Barrick, R.E., Showers, W.J., 1994. Thermophysiology of *Tyrannosaurus rex*: Evidence from Oxygen Isotopes. Science 265, 222–224. https://doi.org/10.1126/science.265.5169.222

Berger, J.-F., Bravard, J.-P., 2012. Le développement économique romain face à la crise environnementale : le cas de la Gaule narbonnaise. Des climats et des hommes. La Découverte, Paris 269–289.

Bernard, A., Daux, V., Lécuyer, C., Brugal, J.-P., Genty, D., Wainer, K., Gardien, V., Fourel, F., Jaubert, J., 2009. Pleistocene seasonal temperature variations recorded in the $\delta^{18}O$ of *Bison priscus* teeth. Earth and Planetary Science Letters 283, 133–143. https://doi.org/10.1016/j.epsl.2009.04.005

Bernard, A., Lécuyer, C., Vincent, P., Amiot, R., Bardet, N., Buffetaut, E., Cuny, G., Fourel, F., Martineau, F., Mazin, J.-M., Prieur, A., 2010. Regulation of body temperature by some mesozoic marine reptiles. Science 328, 1379–1382. https://doi.org/10.1126/science.1187443

Blake, R.E., O'Neil, J.R., Garcia, G.A., 1997. Oxygen isotope systematics of biologically mediated reactions of phosphate: I. Microbial degradation of organophosphorus compounds. Geochimica et Cosmochimica Acta 61, 4411–4422. https://doi.org/10.1016/S0016-7037(97)00272-X

Bond, G., Kromer, B., Beer, J., Muscheler, R., Evans, M.N., Showers, W., Hoffmann, S., Lotti-Bond, R., Hajdas, I., Bonani, G., 2001. Persistent Solar Influence on North Atlantic Climate During the Holocene. Science 294, 2130–2136. https://doi.org/10.1126/science.1065680

Bookman, R., Enzel, Y., Agnon, A., Stein, M., 2004. Late Holocene lake levels of the Dead Sea. GSA Bulletin 116, 555–571. https://doi.org/10.1130/B25286.1

Bowen, G.J., 2020. The Online Isotopes in Precipitation Calculator, version 3.1 [WWW Document]. URL http://www.waterisotopes.org

566 Bowen, G.J., Revenaugh, J., 2003. Interpolating the isotopic composition of modern meteoric
567 precipitation. Water Resources Research 39. https://doi.org/10.1029/2003WR002086
568 Brettell, R., Montgomery, J., Evans, J., 2012. Brewing and stewing: the effect of culturally
569 mediated behaviour on the oxygen isotope composition of ingested fluids and the
570 implications for human provenance studies. J. Anal. At. Spectrom. 27, 778–785.
571 https://doi.org/10.1039/C2JA10335D
572 Britton, K., Fuller, B.T., Tütken, T., Mays, S., Richards, M.P., 2015. Oxygen isotope analysis
573 of human bone phosphate evidences weaning age in archaeological populations. American
574 Journal of Physical Anthropology 157, 226–241. https://doi.org/10.1002/ajpa.22704
575 Büntgen, U., Tegel, W., Nicolussi, K., McCormick, M., Frank, D., Trouet, V., Kaplan, J.O.,
576 Herzig, F., Heussner, K.-U., Wanner, H., Luterbacher, J., Esper, J., 2011. 2500 Years of
577 European Climate Variability and Human Susceptibility. Science 331, 578–582.
578 https://doi.org/10.1126/science.1197175
579 Caroli, I., Caldara, M., 2007. Vegetation history of Lago Battaglia (eastern Gargano coast,
580 Apulia, Italy) during the middle-late Holocene. Vegetation History and Archaeobotany 16,
581 317–327.
582 Chenery, C., Müldner, G., Evans, J., Eckardt, H., Lewis, M., 2010. Strontium and stable
583 isotope evidence for diet and mobility in Roman Gloucester, UK. Journal of
584 Archaeological Science 37, 150–163. https://doi.org/10.1016/j.jas.2009.09.025
585 Chesson, L.A., Valenzuela, L.O., O'Grady, S.P., Cerling, T.E., Ehleringer, J.R., 2010. Links
586 between Purchase Location and Stable Isotope Ratios of Bottled Water, Soda, and Beer in
587 the United States. J. Agric. Food Chem. 58, 7311–7316. https://doi.org/10.1021/jf1003539
588 Cisneros, M., Cacho, I., Frigola, J., Canals, M., Martrat, B., Casado, M., Grimalt, J., Pena, L.,
589 Margaritelli, G., Lirer, F., 2016. Sea surface temperature variability in the central-western
590 Mediterranean Sea during the last 2700 years: a multi-proxy and multi-record approach.

591 Combourieu Nebout, N., Peyron, O., Dormoy, I., Desprat, S., Beaudouin, C., Kotthoff, U.,
592 Marret, F., 2009. Rapid climatic variability in the west Mediterranean during the last 25
593 000 years from high resolution pollen data. Climate of the Past 5, 503–521.
594 Craig, H., 1961. Isotopic Variations in Meteoric Waters. Science 133, 1702–1703.
595 https://doi.org/10.1126/science.133.3465.1702
596 Craig, H., Gordon, L.I., 1965. Deuterium and oxygen 18 variations in the ocean and the
597 marine atmosphere.
598 Crowson, R.A., Showers, W.J., Wright, E.K., Hoering, T.C., 1991. Preparation of phosphate
599 samples for oxygen isotope analysis. Anal. Chem. 63, 2397–2400.
600 https://doi.org/10.1021/ac00020a038
601 Csiro, A.P.B., 1983. Solar variability, weather and climate: An update. Quarterly Journal of
602 the Royal Meteorological Society 109, 23–55. https://doi.org/10.1002/qj.49710945903
603 Dahl-Jensen, D., Mosegaard, K., Gundestrup, N., Clow, G.D., Johnsen, S.J., Hansen, A.W.,
604 Balling, N., 1998. Past Temperatures Directly from the Greenland Ice Sheet. Science 282,
605 268–271. https://doi.org/10.1126/science.282.5387.268
606 D'Angela, D., Longinelli, A., 1990. Oxygen isotopes in living mammal's bone phosphate:
607 Further results. Chemical Geology: Isotope Geoscience section 86, 75–82.
608 https://doi.org/10.1016/0168-9622(90)90007-Y
609 Daniel Bryant, J., Luz, B., Froelich, P.N., 1994. Oxygen isotopic composition of fossil horse
610 tooth phosphate as a record of continental paleoclimate. Palaeogeography,
611 Palaeoclimatology, Palaeoecology, Stable Isotope and Trace-Element Geochemistry of
612 Vertebrate Fossils: Interpreting Ancient Diets and Climates 107, 303–316.
613 https://doi.org/10.1016/0031-0182(94)90102-3
614 Dansgaard, W., 1964. Stable isotopes in precipitation. Tellus 16, 436–468.
615 https://doi.org/10.3402/tellusa.v16i4.8993

616 Darling, G., 2006. Isotopes in water, in: Leng, M.J. (Ed.), Isotopes in Palaeoenvironmental
617 Research, Developments in Paleoenvironmental Research. Springer Netherlands,
618 Dordrecht, pp. 1–66. https://doi.org/10.1007/1-4020-2504-1_01
619 Daux, V., LéCuyer, C., Adam, F., Martineau, F., Vimeux, F., 2005. Oxygen isotope
620 composition of human teeth and the record of climate changes in France (Lorraine) during
621 the last 1700 years. Climatic change 70, 445–464.
622 Daux, V., Lécuyer, C., Héran, M.-A., Amiot, R., Simon, L., Fourel, F., Martineau, F.,
623 Lynnerup, N., Reychler, H., Escarguel, G., 2008. Oxygen isotope fractionation between
624 human phosphate and water revisited. Journal of human evolution 55, 1138–1147.
625 Dermody, B., De Boer, H.J., Bierkens, M.F.P., Weber, S.L., Wassen, M.J., Dekker, S.C.,
626 2012. A seesaw in Mediterranean precipitation during the Roman Period linked to
627 millennial-scale changes in the North Atlantic. Climate of the Past 8, 637–651.
628 Desprat, S., Goñi, M.F.S., Loutre, M.-F., 2003. Revealing climatic variability of the last three
629 millennia in northwestern Iberia using pollen influx data. Earth and Planetary Science
630 Letters 213, 63–78.
631 Drake, B.L., 2012. The influence of climatic change on the Late Bronze Age Collapse and the
632 Greek Dark Ages. Journal of Archaeological Science 39, 1862–1870.
633 https://doi.org/10.1016/j.jas.2012.01.029
634 Eberhardt, L.L., 1969. Similarity, allometry and food chains. Journal of Theoretical Biology
635 24, 43–55. https://doi.org/10.1016/S0022-5193(69)80005-6
636 Esper, J., Büntgen, U., Timonen, M., Frank, D.C., 2012. Variability and extremes of northern
637 Scandinavian summer temperatures over the past two millennia. Global and Planetary
638 Change 88, 1–9.
639 Fagan, B., 2008. The Great Warming: Climate Change and the Rise and Fall of Civilizations.
640 Bloomsbury Publishing USA.

641 Ferrio, J.P., Alonso, N., López, J.B., Araus, J.L., Voltas, J., 2006. Carbon isotope composition
642 of fossil charcoal reveals aridity changes in the NW Mediterranean Basin. Global Change
643 Biology 12, 1253–1266.
644 Fourel, F., Martineau, F., Lécuyer, C., Kupka, H.-J., Lange, L., Ojeimi, C., Seed, M., 2011.
645 $^{18}O/^{16}O$ ratio measurements of inorganic and organic materials by elemental analysis–
646 pyrolysis–isotope ratio mass spectrometry continuous-flow techniques. Rapid
647 Communications in Mass Spectrometry 25, 2691–2696. https://doi.org/10.1002/rcm.5056
648 Fricke, H.C., O'Neil, J.R., 1999. The correlation between $^{18}O/^{16}O$ ratios of meteoric water and
649 surface temperature: its use in investigating terrestrial climate change over geologic time.
650 Earth and Planetary Science Letters 170, 181–196. https://doi.org/10.1016/S0012-
651 821X(99)00105-3
652 Frisia, S., Borsato, A., Spötl, C., Villa, I.M., Cucchi, F., 2005. Climate variability in the SE
653 Alps of Italy over the past 17 000 years reconstructed from a stalagmite record. Boreas 34,
654 445–455.
655 Frumkin, A., Magaritz, M., Carmi, I., Zak, I., 1991. The Holocene climatic record of the salt
656 caves of Mount Sedom Israel. The Holocene 1, 191–200.
657 https://doi.org/10.1177/095968369100100301
658 Gat, J.R., 1996. Oxygen and Hydrogen Isotopes in the Hydrologic Cycle. Annual Review of
659 Earth and Planetary Sciences 24, 225–262. https://doi.org/10.1146/annurev.earth.24.1.225
660 Glimcher, M.J., 2006. Bone: Nature of the Calcium Phosphate Crystals and Cellular,
661 Structural, and Physical Chemical Mechanisms in Their Formation. Reviews in
662 Mineralogy and Geochemistry 64, 223–282. https://doi.org/10.2138/rmg.2006.64.8
663 Haigh, J.D., 2007. The Sun and the Earth's Climate. Living Rev. Sol. Phys. 4, 2.
664 https://doi.org/10.12942/lrsp-2007-2

Halas, S., Skrzypek, G., Meier- Augenstein, W., Pelc, A., Kemp, H.F., 2011. Inter-laboratory calibration of new silver orthophosphate comparison materials for the stable oxygen isotope analysis of phosphates. Rapid Communications in Mass Spectrometry 25, 579–584. https://doi.org/10.1002/rcm.4892

Heim, C., Nowaczyk, N.R., Negendank, J.F., Leroy, S.A., Ben-Avraham, Z., 1997. Near East desertification: evidence from the Dead Sea. Naturwissenschaften 84, 398–401.

Holzhauser, H., Magny, M., Zumbuühl, H.J., 2005. Glacier and lake-level variations in west-central Europe over the last 3500 years. The Holocene 15, 789–801.

Hut, G., 1987. Consultants' group meeting on stable isotope reference samples for geochemical and hydrological investigations.

IAEA/WMO, 2015. Global Network of Isotopes in Precipitation. The GNIP Database. [WWW Document]. URL https://nucleus.iaea.org/wiser

Issar, A.S., Yakir, D., 1997. Isotopes from Wood Buried in the Roman Siege Ramp of Masada: The Roman Period's Colder Climate. The Biblical Archaeologist 60, 101–106. https://doi.org/10.2307/3210599

Jay, M., Richards, M.P., 2006. Diet in the Iron Age cemetery population at Wetwang Slack, East Yorkshire, UK: carbon and nitrogen stable isotope evidence. Journal of Archaeological Science 33, 653–662. https://doi.org/10.1016/j.jas.2005.09.020

Jiang, H., Eiríksson, J., Schulz, M., Knudsen, K.-L., Seidenkrantz, M.-S., 2005. Evidence for solar forcing of sea-surface temperature on the North Icelandic Shelf during the late Holocene. Geology 33, 73–76. https://doi.org/10.1130/G21130.1

Kaniewski, D., Paulissen, E., Campo, E.V., Weiss, H., Otto, T., Bretschneider, J., Lerberghe, K.V., 2010. Late second–early first millennium BC abrupt climate changes in coastal Syria and their possible significance for the history of the Eastern Mediterranean. Quaternary Research 74, 207–215. https://doi.org/10.1016/j.yqres.2010.07.010

690 Kohn, M.J., 1996. Predicting animal $\delta^{18}O$: Accounting for diet and physiological adaptation.
691 Geochimica et Cosmochimica Acta 60, 4811–4829. https://doi.org/10.1016/S0016-
692 7037(96)00240-2
693 Kottek, M., Grieser, J., Beck, C., Rudolf, B., Rubel, F., 2006. World map of the Köppen-
694 Geiger climate classification updated. Meteorologische Zeitschrift 15, 259–263.
695 Lamb, A.L., Evans, J.E., Buckley, R., Appleby, J., 2014. Multi-isotope analysis demonstrates
696 significant lifestyle changes in King Richard III. Journal of Archaeological Science 50,
697 559–565. https://doi.org/10.1016/j.jas.2014.06.021
698 Lamb, H.H., 1995. Climate, History and the Modern World. Psychology Press.
699 Le Béchennec, Y., Frère, S., Corsiez, A., Rolland, J., Sauvageot, P., 2016. Rapport final
700 d'opération : Thézy-Glimont, Les Vergnes, (Somme). Novembre 2012 - Mai 2013. Service
701 Archéologie Préventive d'Amiens Métropole.
702 Lécuyer, C., 2013. Water on Earth, 1st ed. John Wiley & Sons, Ltd.
703 https://doi.org/10.1002/9781118574928
704 Lécuyer, C., Atrops, F., Amiot, R., Angst, D., Daux, V., Flandrois, J.-P., Fourel, F., Rey, K.,
705 Royer, A., Seris, M., Touzeau, A., Rousseau, D., 2018. Tsunami sedimentary deposits of
706 Crete records climate during the 'Minoan Warming Period' (≈3350 yr BP). The Holocene
707 28, 914–929. https://doi.org/10.1177/0959683617752840
708 Lécuyer, C., Fourel, F., Martineau, F., Amiot, R., Bernard, A., Daux, V., Escarguel, G.,
709 Morrison, J., 2007. High-precision determination of $^{18}O/^{16}O$ ratios of silver phosphate by
710 EA-pyrolysis-IRMS continuous flow technique. Journal of Mass Spectrometry 42, 36–41.
711 https://doi.org/10.1002/jms.1130
712 Lécuyer, C., Grandjean, P., O'Neil, J.R., Cappetta, H., Martineau, F., 1993. Thermal
713 excursions in the ocean at the Cretaceous—Tertiary boundary (northern Morocco): $\delta^{18}O$

714 record of phosphatic fish debris. Palaeogeography, Palaeoclimatology, Palaeoecology 105,
715 235–243. https://doi.org/10.1016/0031-0182(93)90085-W
716 Lécuyer, C., Grandjean, P., Sheppard, S.M.F., 1999. Oxygen isotope exchange between
717 dissolved phosphate and water at temperatures ≤135°C: inorganic versus biological
718 fractionations. Geochimica et Cosmochimica Acta 63, 855–862.
719 https://doi.org/10.1016/S0016-7037(99)00096-4
720 LeGeros, R., 1981. Apatites in biological systems. Progress in Crystal Growth and
721 Characterization 4, 1–45. https://doi.org/10.1016/0146-3535(81)90046-0
722 Lightfoot, E., O'Connell, T.C., 2016. On the Use of Biomineral Oxygen Isotope Data to
723 Identify Human Migrants in the Archaeological Record: Intra-Sample Variation, Statistical
724 Methods and Geographical Considerations. PLoS One 11.
725 https://doi.org/10.1371/journal.pone.0153850
726 Lirer, F., Sprovieri, M., Vallefuoco, M., Ferraro, L., Pelosi, N., Giordano, L., Capotondi, L.,
727 2014. Planktonic foraminifera as bio-indicators for monitoring the climatic changes that
728 have occurred over the past 2000 years in the southeastern Tyrrhenian Sea. Integrative
729 Zoology 9, 542–554. https://doi.org/10.1111/1749-4877.12083
730 Lockwood, M., 2012. Solar Influence on Global and Regional Climates. Surv Geophys 33,
731 503–534. https://doi.org/10.1007/s10712-012-9181-3
732 Longin, R., 1971. New Method of Collagen Extraction for Radiocarbon Dating. Nature 230,
733 241–242. https://doi.org/10.1038/230241a0
734 Longinelli, A., 1984. Oxygen isotopes in mammal bone phosphate: A new tool for
735 paleohydrological and paleoclimatological research? Geochimica et Cosmochimica Acta
736 48, 385–390. https://doi.org/10.1016/0016-7037(84)90259-X

737 Luterbacher, J., Werner, J.P., Smerdon, J.E., Fernández-Donado, L., González-Rouco, F.J.,
738 Barriopedro, D., Ljungqvist, F.C., Büntgen, U., Zorita, E., Wagner, S., 2016. European
739 summer temperatures since Roman times. Environmental research letters 11, 024001.
740 Luz, B., Kolodny, Y., 1985. Oxygen isotope variations in phosphate of biogenic apatites, IV.
741 Mammal teeth and bones. Earth and Planetary Science Letters 75, 29–36.
742 https://doi.org/10.1016/0012-821X(85)90047-0
743 Luz, B., Kolodny, Y., Horowitz, M., 1984. Fractionation of oxygen isotopes between
744 mammalian bone-phosphate and environmental drinking water. Geochimica et
745 Cosmochimica Acta 48, 1689–1693. https://doi.org/10.1016/0016-7037(84)90338-7
746 Magny, M., de Beaulieu, J.-L., Drescher-Schneider, R., Vannière, B., Walter-Simonnet, A.-
747 V., Miras, Y., Millet, L., Bossuet, G., Peyron, O., Brugiapaglia, E., Leroux, A., 2007.
748 Holocene climate changes in the central Mediterranean as recorded by lake-level
749 fluctuations at Lake Accesa (Tuscany, Italy). Quaternary Science Reviews 26, 1736–1758.
750 https://doi.org/10.1016/j.quascirev.2007.04.014
751 Mangini, A., Spötl, C., Verdes, P., 2005. Reconstruction of temperature in the Central Alps
752 during the past 2000 yr from a $\delta^{18}O$ stalagmite record. Earth and Planetary Science Letters
753 235, 741–751. https://doi.org/10.1016/j.epsl.2005.05.010
754 Margaritelli, G., Vallefuoco, M., Di Rita, F., Capotondi, L., Bellucci, L.G., Insinga, D.D.,
755 Petrosino, P., Bonomo, S., Cacho, I., Cascella, A., Ferraro, L., Florindo, F., Lubritto, C.,
756 Lurcock, P.C., Magri, D., Pelosi, N., Rettori, R., Lirer, F., 2016. Marine response to
757 climate changes during the last five millennia in the central Mediterranean Sea. Global and
758 Planetary Change 142, 53–72. https://doi.org/10.1016/j.gloplacha.2016.04.007
759 Marquer, L., Pomel, S., Abichou, A., Schulz, E., Kaniewski, D., Campo, E.V., 2008. Late
760 Holocene high resolution palaeoclimatic reconstruction inferred from Sebkha Mhabeul,

761 southeast Tunisia. Quaternary Research 70, 240–250.
762 https://doi.org/10.1016/j.yqres.2008.06.002
763 Martin, C., Maureille, B., Amiot, R., Touzeau, A., Royer, A., Fourel, F., Panczer, G.,
764 Flandrois, J.-P., Lécuyer, C., 2017. Record of Nile seasonality in Nubian neonates.
765 Isotopes in environmental and health studies 53, 223–242.
766 McCormick, M., Büntgen, U., Cane, M.A., Cook, E.R., Harper, K., Huybers, P., Litt, T.,
767 Manning, S.W., Mayewski, P.A., More, A.F.M., Nicolussi, K., Tegel, W., 2012. Climate
768 Change during and after the Roman Empire: Reconstructing the Past from Scientific and
769 Historical Evidence. The Journal of Interdisciplinary History 43, 169–220.
770 https://doi.org/10.1162/JINH_a_00379
771 McDermott, F., Mattey, D.P., Hawkesworth, C., 2001. Centennial-Scale Holocene Climate
772 Variability Revealed by a High-Resolution Speleothem $\delta^{18}O$ Record from SW Ireland.
773 Science 294, 1328–1331. https://doi.org/10.1126/science.1063678
774 Migowski, C., Stein, M., Prasad, S., Negendank, J.F.W., Agnon, A., 2006. Holocene Climate
775 Variability and Cultural Evolution in the Near East from the Dead Sea Sedimentary
776 Record. Quaternary Research 66, 421–431. https://doi.org/10.1016/j.yqres.2006.06.010
777 Moreau, C., Caffy, I., Comby, C., Delqué-Količ, E., Dumoulin, J.-P., Hain, S., Quiles, A.,
778 Setti, V., Souprayen, C., Thellier, B., Vincent, J., 2013. Research and Development of the
779 Artemis 14C AMS Facility: Status Report. Radiocarbon 55, 331–337.
780 https://doi.org/10.1017/S0033822200057441
781 Négrel, Ph., Petelet-Giraud, E., 2005. Strontium isotopes as tracers of groundwater-induced
782 floods: the Somme case study (France). Journal of Hydrology 305, 99–119.
783 https://doi.org/10.1016/j.jhydrol.2004.08.031

784 Nesje, A., Lie, Ø., Dahl, S.O., 2000. Is the North Atlantic Oscillation reflected in
785 Scandinavian glacier mass balance records? Journal of Quaternary Science 15, 587–601.
786 https://doi.org/10.1002/1099-1417(200009)15:6<587::AID-JQS533>3.0.CO;2-2
787 Neukom, R., Steiger, N., Gómez-Navarro, J.J., Wang, J., Werner, J.P., 2019. No evidence for
788 globally coherent warm and cold periods over the preindustrial Common Era. Nature 571,
789 550–554. https://doi.org/10.1038/s41586-019-1401-2
790 Oldenborgh, G.J. van, Laat, A.T.J. de, Luterbacher, J., Ingram, W.J., Osborn, T.J., 2013.
791 Claim of solar influence is on thin ice: are 11-year cycle solar minima associated with
792 severe winters in Europe? Environ. Res. Lett. 8, 024014. https://doi.org/10.1088/1748-
793 9326/8/2/024014
794 Piva, A., Asioli, A., Trincardi, F., Schneider, R.R., Vigliotti, L., 2008. Late-Holocene climate
795 variability in the Adriatic Sea (Central Mediterranean). The Holocene 18, 153–167.
796 https://doi.org/10.1177/0959683607085606
797 Prowse, T., Schwarcz, H.P., Saunders, S., Macchiarelli, R., Bondioli, L., 2004. Isotopic
798 paleodiet studies of skeletons from the Imperial Roman-age cemetery of Isola Sacra,
799 Rome, Italy. Journal of Archaeological Science 31, 259–272.
800 https://doi.org/10.1016/j.jas.2003.08.008
801 Reimer, P.J., Bard, E., Bayliss, A., Beck, J.W., Blackwell, P.G., Ramsey, C.B., Buck, C.E.,
802 Cheng, H., Edwards, R.L., Friedrich, M., Grootes, P.M., Guilderson, T.P., Haflidason, H.,
803 Hajdas, I., Hatté, C., Heaton, T.J., Hoffmann, D.L., Hogg, A.G., Hughen, K.A., Kaiser,
804 K.F., Kromer, B., Manning, S.W., Niu, M., Reimer, R.W., Richards, D.A., Scott, E.M.,
805 Southon, J.R., Staff, R.A., Turney, C.S.M., Plicht, J. van der, 2013. IntCal13 and Marine13
806 Radiocarbon Age Calibration Curves 0–50,000 Years cal BP. Radiocarbon 55, 1869–1887.
807 https://doi.org/10.2458/azu_js_rc.55.16947

Richardin, P., Porcier, S., Ikram, S., Louarn, G., Berthet, D., 2017. Cats, Crocodiles, Cattle, and More: Initial Steps Toward Establishing a Chronology of Ancient Egyptian Animal Mummies. Radiocarbon 59, 595–607. https://doi.org/10.1017/RDC.2016.102

Roberts, N., Reed, J.M., Leng, M.J., Kuzucuoğlu, C., Fontugne, M., Bertaux, J., Woldring, H., Bottema, S., Black, S., Hunt, E., Karabiyikoğlu, M., 2001. The tempo of Holocene climatic change in the eastern Mediterranean region: new high-resolution crater-lake sediment data from central Turkey. The Holocene 11, 721–736. https://doi.org/10.1191/09596830195744

Rozanski, K., Araguás-Araguás, L., Gonfiantini, R., 1993. Isotopic patterns in modern global precipitation. Climate change in continental isotopic records 78, 1–36.

Rozanski, K., Araguás-Araguás, L., Gonfiantini, R., 1992. Relation Between Long-Term Trends of Oxygen-18 Isotope Composition of Precipitation and Climate. Science 258, 981–985. https://doi.org/10.1126/science.258.5084.981

Schilman, B., Bar-Matthews, M., Almogi-Labin, A., Luz, B., 2001. Global climate instability reflected by Eastern Mediterranean marine records during the late Holocene. Palaeogeography, Palaeoclimatology, Palaeoecology 176, 157–176. https://doi.org/10.1016/S0031-0182(01)00336-4

Seidenkrantz, M.-S., Aagaard-Sørensen, S., Sulsbrück, H., Kuijpers, A., Jensen, K.G., Kunzendorf, H., 2007. Hydrography and climate of the last 4400 years in a SW Greenland fjord: implications for Labrador Sea palaeoceanography. The Holocene 17, 387–401. https://doi.org/10.1177/0959683607075840

Séon, N., Amiot, R., Martin, J.E., Young, M.T., Middleton, H., Fourel, F., Picot, L., Valentin, X., Lécuyer, C., 2020. Thermophysiologies of Jurassic marine crocodylomorphs inferred from the oxygen isotope composition of their tooth apatite. Philosophical Transactions of

the Royal Society B: Biological Sciences 375, 20190139. https://doi.org/10.1098/rstb.2019.0139

Shimamoto, H., Komiya, S., 2000. The turnover of body water as an indicator of health. J Physiol Anthropol Appl Human Sci 19, 207–212. https://doi.org/10.2114/jpa.19.207

Smith, A.C., Wynn, P.M., Barker, P.A., Leng, M.J., Noble, S.R., Tych, W., 2016. North Atlantic forcing of moisture delivery to Europe throughout the Holocene. Scientific Reports 6, 1–7. https://doi.org/10.1038/srep24745

Taricco, C., Ghil, M., Alessio, S.M., Vivaldo, G., 2009. Two millennia of climate variability in the Central Mediterranean 5, 171–181. https://doi.org/10.5194/cp-5-171-2009

Tinner, W., Lotter, A.F., Ammann, B., Conedera, M., Hubschmid, P., van Leeuwen, J.F.N., Wehrli, M., 2003. Climatic change and contemporaneous land-use phases north and south of the Alps 2300 BC to 800 AD. Quaternary Science Reviews 22, 1447–1460. https://doi.org/10.1016/S0277-3791(03)00083-0

Touzeau, A., Blichert-Toft, J., Amiot, R., Fourel, F., Martineau, F., Cockitt, J., Hall, K., Flandrois, J.-P., Lécuyer, C., 2013. Egyptian mummies record increasing aridity in the Nile valley from 5500 to 1500 yr before present. Earth and Planetary Science Letters 375, 92–100.

Tütken, T., Vennemann, T.W., 2011. Fossil bones and teeth: Preservation or alteration of biogenic compositions? Palaeogeography, Palaeoclimatology, Palaeoecology 1–2, 1–8. https://doi.org/10.1016/j.palaeo.2011.06.020

von Grafenstein, U., Erlenkeuser, H., Müller, J., Trimborn, P., Alefs, J., 1996. A 200-year mid-European air temperature record preserved in lake sediments: An extension of the δ^{18}Op-air temperature relation into the past. Geochimica et Cosmochimica Acta 60, 4025–4036. https://doi.org/10.1016/S0016-7037(96)00230-X

Wang, T., Surge, D., Mithen, S., 2012. Seasonal temperature variability of the Neoglacial (3300–2500BP) and Roman Warm Period (2500–1600BP) reconstructed from oxygen isotope ratios of limpet shells (Patella vulgata), Northwest Scotland. Palaeogeography, Palaeoclimatology, Palaeoecology 317–318, 104–113. https://doi.org/10.1016/j.palaeo.2011.12.016

Wick, L., Lemcke, G., Sturm, M., 2003. Evidence of Lateglacial and Holocene climatic change and human impact in eastern Anatolia: high-resolution pollen, charcoal, isotopic and geochemical records from the laminated sediments of Lake Van, Turkey. The Holocene 13, 665–675. https://doi.org/10.1191/0959683603hl653rp

Wopenka, B., Pasteris, J.D., 2005. A mineralogical perspective on the apatite in bone. Materials Science and Engineering: C, NATO Advanced Study Institute (ASI on Learning from Nature How to design New Implantable Biomaterials: From Biomineralization Fundamentals to Biomimetic Materials and Processing Routes) 25, 131–143. https://doi.org/10.1016/j.msec.2005.01.008

Zanchetta, G., Drysdale, R.N., Hellstrom, J.C., Fallick, A.E., Isola, I., Gagan, M.K., Pareschi, M.T., 2007. Enhanced rainfall in the Western Mediterranean during deposition of sapropel S1: stalagmite evidence from Corchia cave (Central Italy). Quaternary Science Reviews 26, 279–286. https://doi.org/10.1016/j.quascirev.2006.12.003

Tables

Table 1: Grave, nature, identification and corresponding dates (at 95.4% certainty) inferred from ^{14}C dating of the samples from Thézy-Glimont. The archaeological data come from Le Béchennec et al. (2016).

* corresponds to the three individuals for which various bones were sampled, see Figure 2.

§: If there are two or three dates from the same sample, the radiocarbon dates have been combined before calibration. Such a combination is checked for internal consistency by a chi-squared test which is performed automatically by the OxCal™ program.

Figures

Figure 1: (a) Geographic map of France with the location of the Gallic site of Thézy-Glimont, Picardie, France. PM = Prime Meridian. The datum used for latitude and longitude is WGS84. Picture was taken from Google Earth™. (b) General plan of the archaeological site. 1: Area where the excavated graves are located. 2: Intermediate area. 3: Enclosure with iron furniture and weapons. In gray is represented a trench from World War 1 (1918). The background image was taken from Google Maps™.

Figure 2: Sampling points and intra-skeletal $\delta^{18}O_p$ (‰, V-SMOW) variations represented as local deviation from the average $\delta^{18}O_p$ value of bones coming from TG-01, TG-02 and TG-03 individuals.

Figure 3: $\delta^{18}O_p$ (‰, V-SMOW) values of bones (blue squares) and teeth (red triangles) from humans and animals of Thézy-Glimont. Bones and teeth which are aligned vertically correspond to a same individual. Humans, bovids and horses are represented by increasing sample number from left to right.

Figure 4: Comparison of oxygen isotope fractionation equations between apatite phosphate ($\delta^{18}O_p$, ‰, V-SMOW) and drinking water ($\delta^{18}O_w$, ‰, V-SMOW) proposed by Daux et al.

(2008) for humans, Longinelli (1984) for pigs, D'Angela and Longinelli (1990) for bovids and Bryant et al. (1994) for horses.

Figure 5: $\delta^{18}O_w$ values (‰, V-SMOW) of drinking water inferred from the bones of humans and animals from Thézy-Glimont. Humans and bovids are represented by increasing sample number from left to right. Error bars represent the total uncertainties. The red dashed lines represent the modern $\delta^{18}O_w$ values measured in the Avre river by Négrel and Petelet-Giraud (2005) in April (A) and October (O) 2001.

Figure 6: Reconstructed Mean Annual Temperatures (MAT) inferred from the oxygen isotope composition of drinking water, using the oxygen isotope fractionation equation of von Grafenstein et al. (1996) (blue squares) and Lécuyer (2013) (red triangles). Humans and bovids are represented by increasing sample number from left to right. The horizontal dashed line corresponds to the modern yearly MAT in Picardie, France, averaged throughout the years 1980 to 2010 (data from Météo France™).

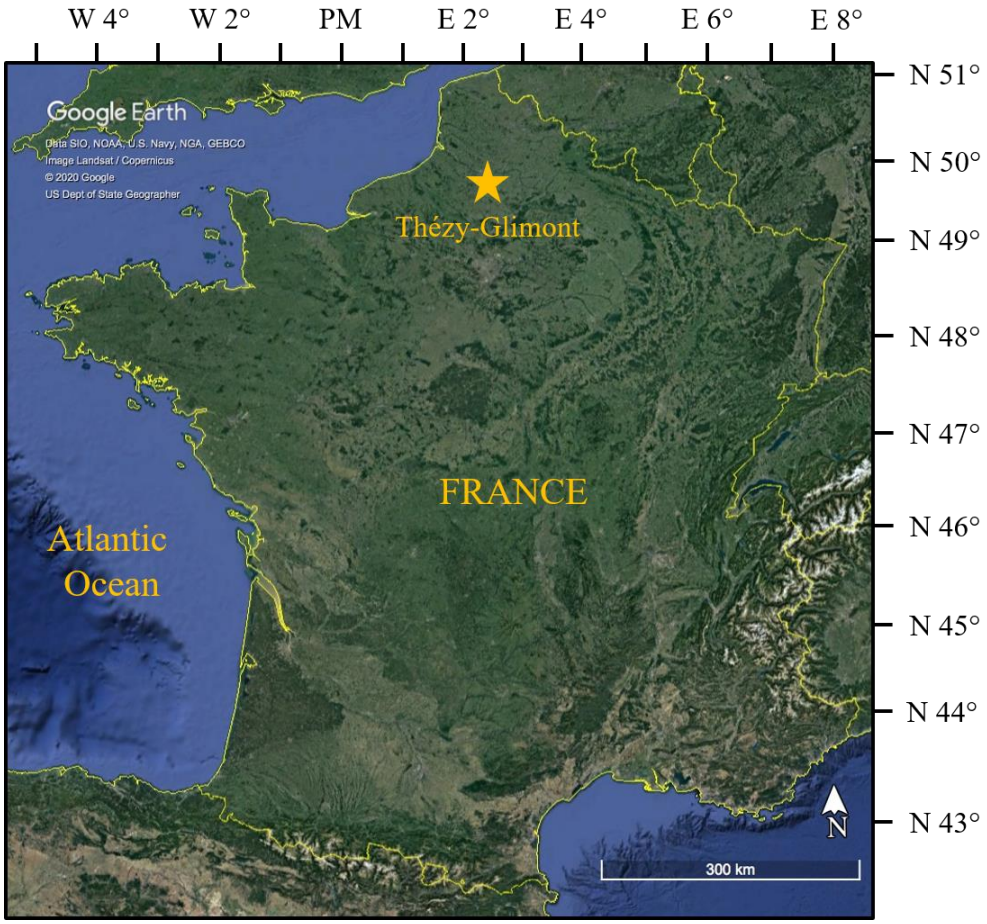
W 4°
W 2°
PM
E 2°
E 4°
E 6°
E 8°
N 51°
N 50°
N 49°
N 48°
N 47°
N 46°
N 45°
N 44°
N 43°
Google Earth
Data SIO, NOAA, U.S. Navy, NGA, GEBCO
Image Landsat / Copernicus
© 2020 Google
US Dept of State Geographer
Thézy-Glimont
FRANCE
Atlantic
Ocean
N
300 km

(a)

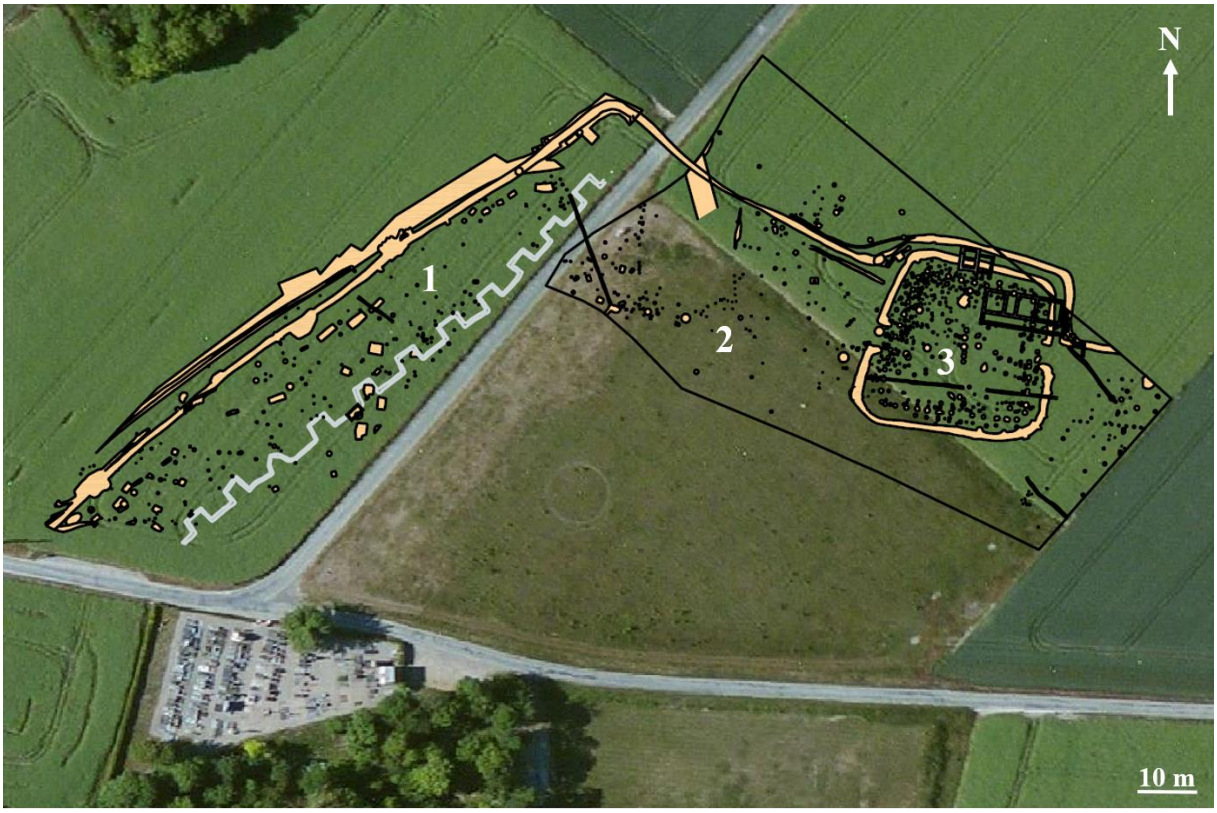
N
1
2
3
10 m

(b)

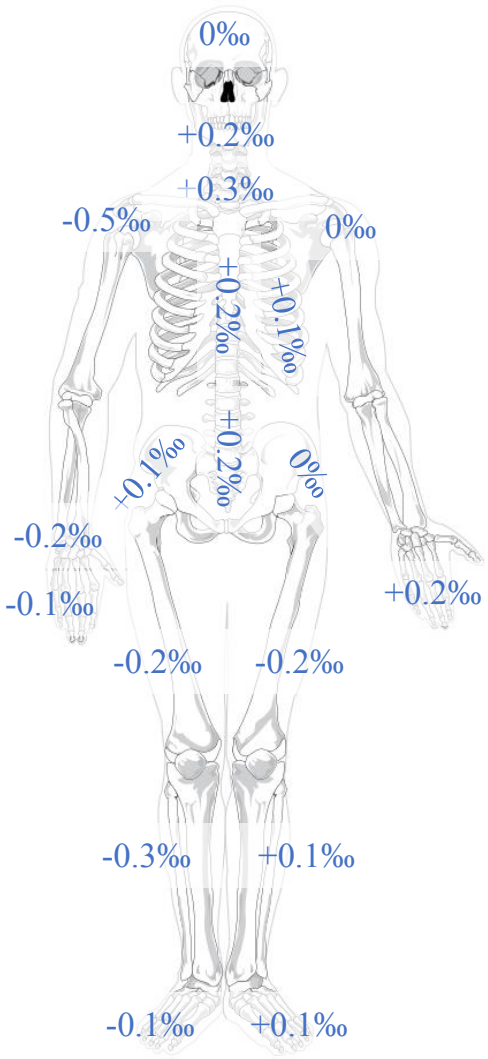

TG-01

Mean $\delta^{18}O_p$ (V-SMOW): 16.6‰

Standard Deviation: 0.2‰

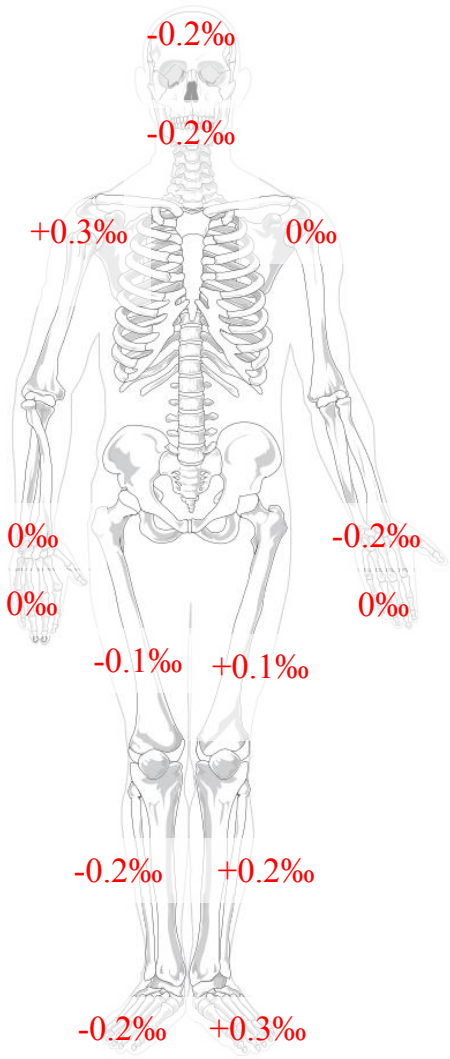

TG-02

Mean $\delta^{18}O_p$ (V-SMOW): 17.6‰

Standard Deviation: 0.2‰

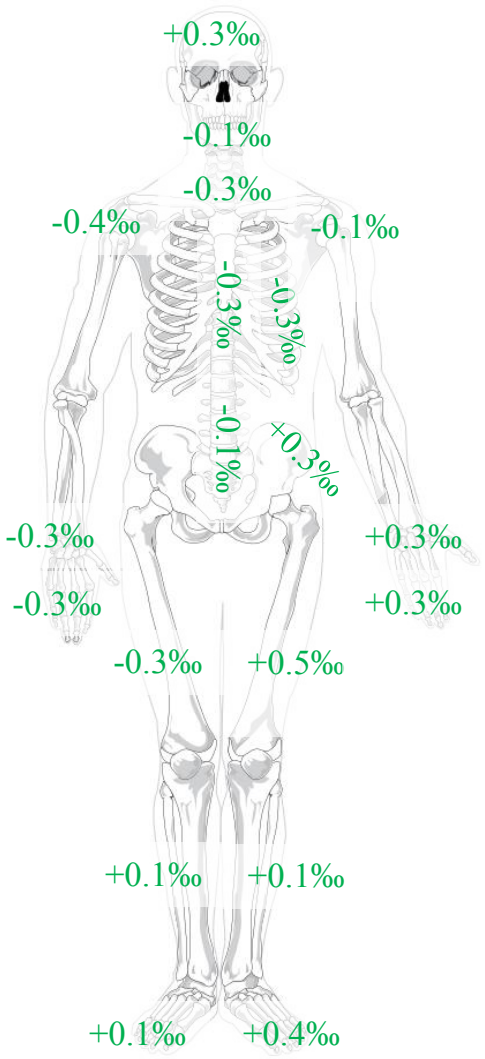

TG-03

Mean $\delta^{18}O_p$ (V-SMOW): 16.8‰

Standard Deviation: 0.3‰

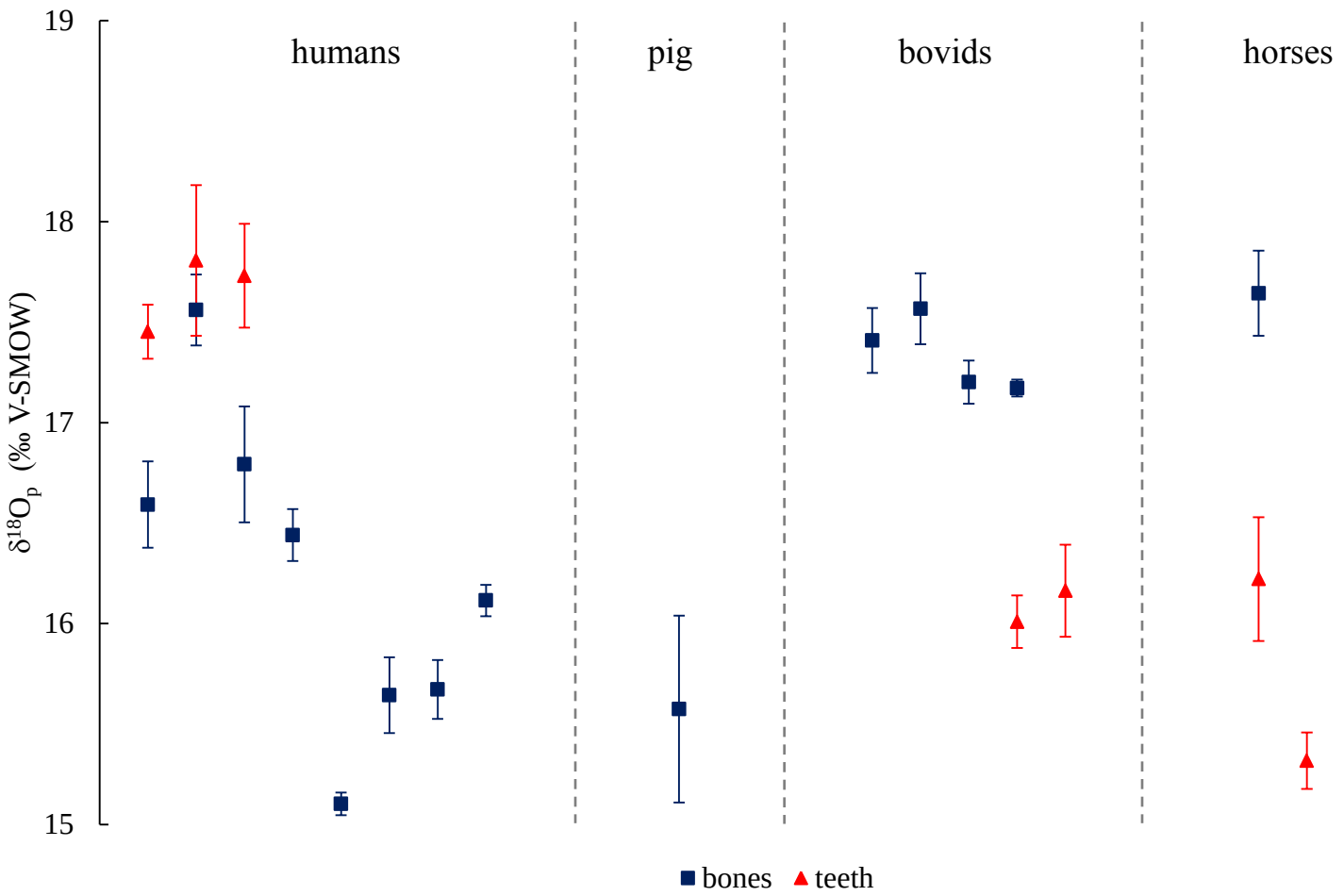
19
18
17
16
15
δ18Op (‰ V-SMOW)
humans
pig
bovids
horses
bones
teeth

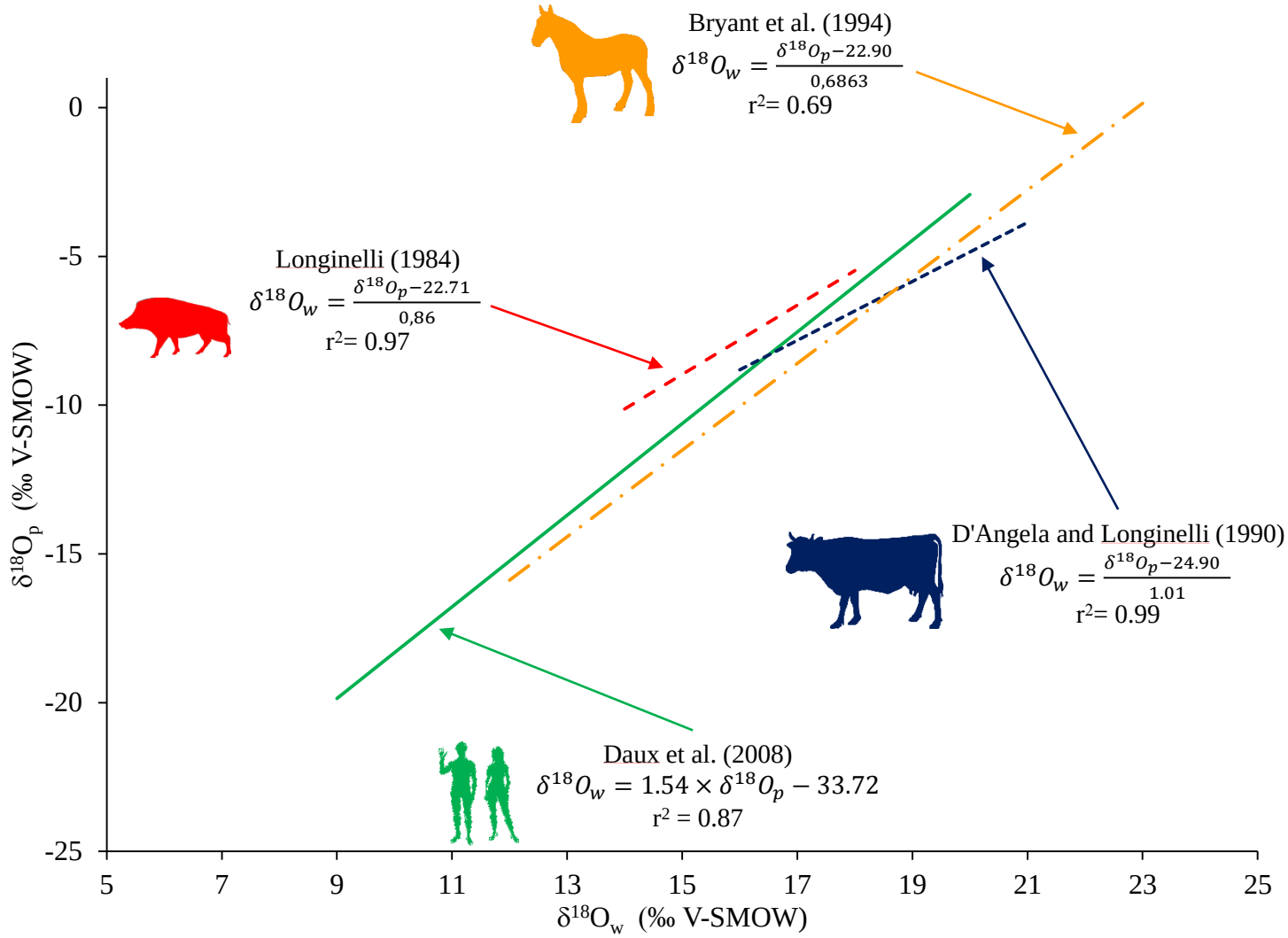
Bryant et al. (1994)
$\delta^{18}O_w = \frac{\delta^{18}O_p - 22.90}{0,6863}$
r²= 0.69
Longinelli (1984)
$\delta^{18}O_w = \frac{\delta^{18}O_p - 22.71}{0,86}$
r²= 0.97
D'Angela and Longinelli (1990)
$\delta^{18}O_w = \frac{\delta^{18}O_p - 24.90}{1.01}$
r²= 0.99
Daux et al. (2008)
$\delta^{18}O_w = 1.54 \times \delta^{18}O_p - 33.72$
r² = 0.87
0
-5
-10
-15
-20
-25
5
7
9
11
13
15
17
19
21
23
25
δ¹⁸O_p (‰ V-SMOW)
δ¹⁸O_w (‰ V-SMOW)

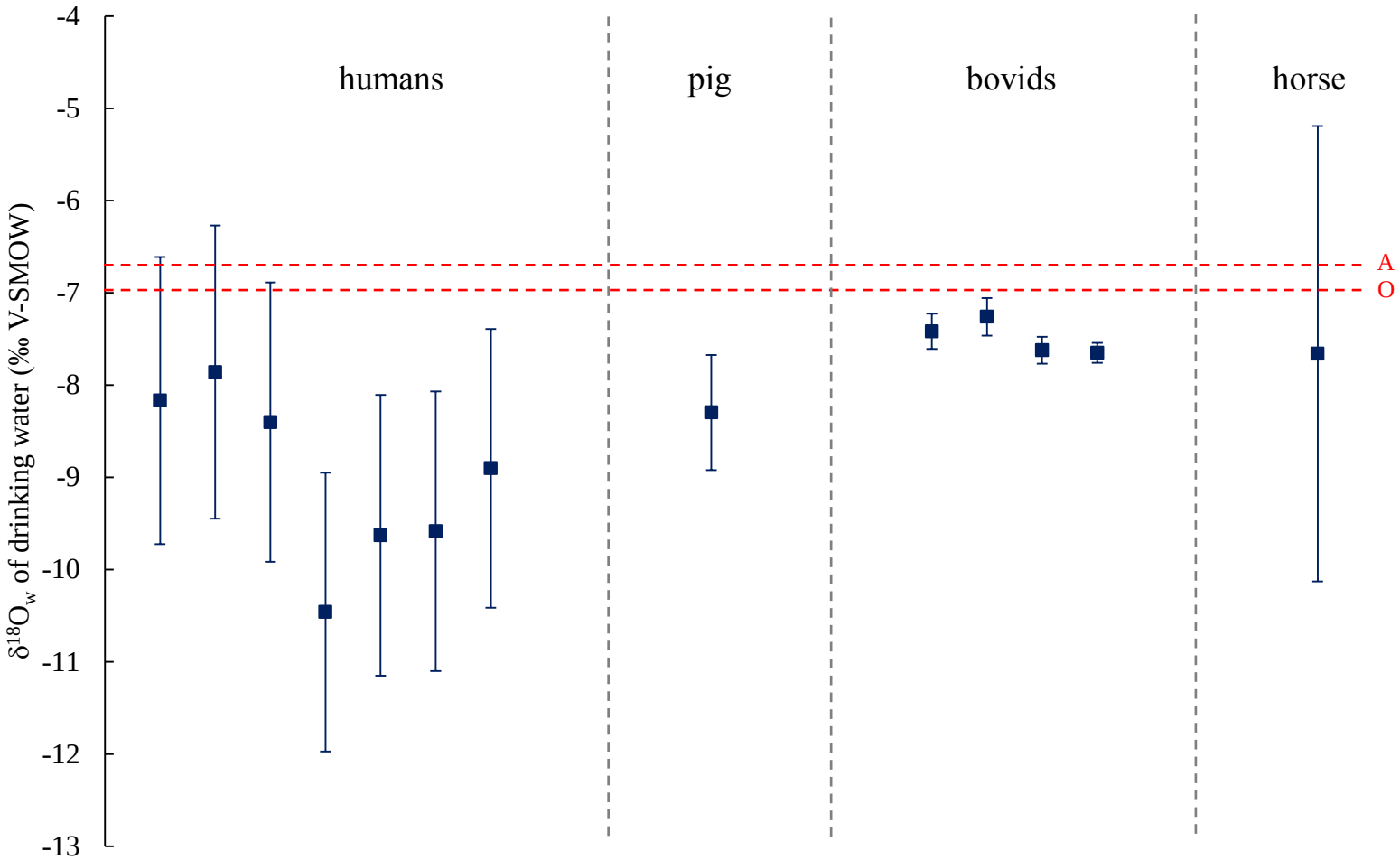
humans
pig
bovids
horse
A
O
-4
-5
-6
-7
-8
-9
-10
-11
-12
-13
δ18Ow of drinking water (‰ V-SMOW)

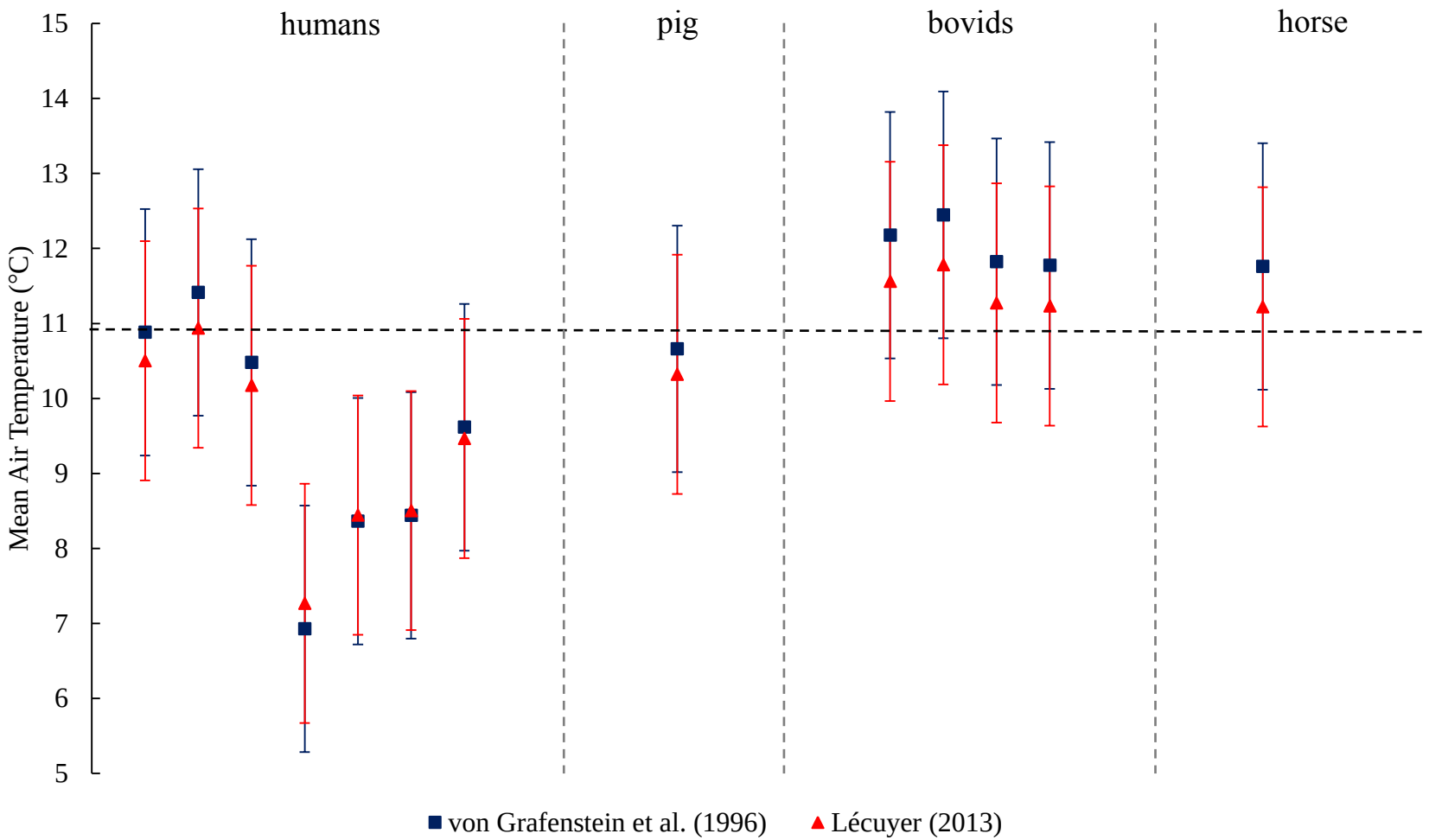
humans
pig
bovids
horse
Mean Air Temperature (°C)
15
14
13
12
11
10
9
8
7
6
5
von Grafenstein et al. (1996)
Lécuyer (2013)

Grave	Individual	Type	Sex	Age (years)	Sample type	^{14}C dates (BP)	Calibrated dates - 2σ (95.4%)[§]
TGV 1135	TG-01	*Homo sapiens*	Male	< 30	*	2160 ± 30 2190 ± 30	358 cal BCE (56.7%) 280 cal BCE 258 cal BCE (2.6%) 243 cal BCE 236 cal BCE (36.1%) 170 cal BCE
					1st premolar (PM1)	-	-
					1st molar (M1)	-	-
					2nd molar (M2)	-	-
	TG-CH1	*Equus caballus*	Male	3	Left phalanx	2130 ± 30	350 cal BCE (10.5%) 308 cal BCE 210 cal BCE (84.9%) 52 cal BCE
					3rd molar (M3)	2150 ± 30 2180 ± 30 2190 ± 30	356 cal BCE (59.0%) 286 cal BCE 234 cal BCE (36.4%) 170 cal BCE
	TG-B1	*Bos taurus*	Female	4	Right phalanx	-	-
	TG-B2	*Bos taurus*	Male	young	Left talus	-	-
	TG-B3	*Bos taurus*	Male	2	Left phalanx	-	-
	TG-B4	*Bos taurus*	Male	4	Left phalanx	-	-
					3rd molar (M3)	2170 ± 30 2205 ± 30	359 cal BCE (59.2%) 274 cal BCE 261 cal BCE (36.2%) 184 cal BCE
	TG-CO1	*Sus scrofa*	Male	-	Right Radius	-	-
					Rib	-	-
					Vertebra	-	-

TGV 1249	TG-02	*Homo sapiens*	Male	15	*	2200 ± 30 2170 ± 30	358 cal BCE (59.2%) 276 cal BCE 260 cal BCE (36.2%) 180 cal BCE
					1st premolar (PM1)	-	-
					1st molar (M1)	-	-
					3rd molar (M3)	-	-
TGV 1450	TG-03	*Homo sapiens*	Male	Adult	*	2185 ± 30	361 cal BCE (95.4%) 172 cal BCE
					1st premolar (PM1)	-	-
					2nd molar (M2)	-	-
					3rd molar (M3)	-	-
TGV 1219	TG-04	*Homo sapiens*	Male	Adult	Right femur	2195 ± 30 2175 ± 30	358 cal BCE (59.0%) 276 cal BCE 260 cal BCE (36.4%) 180 cal BCE
TGV 1138	TG-05	*Homo sapiens*	Male	30 to 59	Right femur	2180 ± 30 2145 ± 30	356 cal BCE (46.7%) 284 cal BCE 256 cal BCE (0.5%) 250 cal BCE 235 cal BCE (46.0%) 156 cal BCE 134 cal BCE (2.1%) 116 cal BCE
	TG-CH2	*Equus caballus*	Male	5	Molar	2120 ± 30 2135 ± 30	344 cal BCE (4.3%) 322 cal BCE 206 cal BCE (87.9%) 88 cal BCE 76 cal BCE (3.2%) 58 cal BCE
TGV 1140	TG-06	*Homo sapiens*	Male	Adult	Right femur	2170 ± 30 2145 ± 30	355 cal BCE (40.5%) 289 cal BCE 232 cal BCE (51.0%) 151 cal BCE 136 cal BCE (3.9%) 114 cal BCE
TGV1206	TG-07	*Homo sapiens*	Male	Adult	Right femur	2200 ± 30 2225 ± 30	364 cal BCE (95.4%) 203 cal BCE
TGV 1246	TG-08	*Homo sapiens*	Male	Adult	Tibia	-	-

TGV 1222	TG-B5	*Bos taurus*	Male	2 to 3	3rd molar	2135 ± 30 2160 ± 30 2115 ± 30	346 cal BCE (8.2%) 320 cal BCE 206 cal BCE (87.2%) 102 cal BCE